

Research Articles | Behavioral/Cognitive

Iron deposition and distribution across the hippocampus is associated with pattern separation and pattern completion in older adults at risk for Alzheimer's disease

<https://doi.org/10.1523/JNEUROSCI.1973-23.2024>

Received: 18 October 2023
Revised: 16 December 2023
Accepted: 3 January 2024

Copyright © 2024 the authors

This Early Release article has been peer reviewed and accepted, but has not been through the composition and copyediting processes. The final version may differ slightly in style or formatting and will contain links to any extended data.

Alerts: Sign up at www.jneurosci.org/alerts to receive customized email alerts when the fully formatted version of this article is published.

1 **Title:** Iron deposition and distribution across the hippocampus is associated with pattern separation
2 and pattern completion in older adults at risk for Alzheimer's disease

3

4 **Abbreviated Title (50 characters max):** Distribution of hippocampal iron and memory in aging

5

6 **Authors:** Jing Zhou ^a, Alfie Wearn ^a, Julia Huck ^{b,k,l}, Colleen Hughes ^a, Giulia Baracchini ^a, Jennifer
7 Tremblay-Mercier ^c, Judes Poirier ^{c,d}, Sylvia Villeneuve ^{a,c,d}, Christine Lucas Tardif ^{a,e,l}, M. Mallar
8 Chakravarty ^{d,e,m}, Ana M. Daugherty ^f, Claudine J. Gauthier ^{b,g}, Gary R. Turner ^h, R. Nathan Spreng
9 ^{a,c,d,i,j,*}

10 for the PREVENT-AD Research Group

11

12 **Affiliations:**

13 ^a Montreal Neurological Institute, McGill University, Montreal, QC, Canada. H3A 2B4

14 ^b Physics Department, Concordia University, Montréal, QC, Concordia University, Montreal, QC,
15 Canada. H4B 1R6

16 ^c StoP-AD Centre, Douglas Mental Health Institute Research Centre, Montreal,
17 QC, Canada. H4H 1R3

18 ^d Department of Psychiatry, McGill University, Montreal, QC, Canada. H3A 1A1

19 ^e Department of Biomedical Engineering, McGill University, Montreal, QC, Canada. H3A 2B4

20 ^f Department of Psychology and Institute of Gerontology, Wayne State University, Detroit, Michigan.
21 48202

22 ^g Montreal Heart Institute, Montreal, QC, Canada, H1T 1C8

23 ^h Department of Psychology, York University, Toronto, ON, Canada. M3J 1P3

24 ⁱ Department of Neurology and Neurosurgery, Montréal Neurological Institute, Montréal, QC, Canada.
25 H3A 1A1

26 ^j Departments of Psychiatry and Psychology, McGill University, Montréal, QC, Canada. H3A 1G1

27 ^k Department of Radiology, Université de Sherbrooke, Sherbrooke, Québec, Canada

28 ^l Sherbrooke Connectivity Imaging Lab (SCIL), Computer Science Department, Faculty of Science,
29 University of Sherbrooke, Canada

30 ^m Cerebral Imaging Centre, Douglas Mental Health Institute Research Centre, Montreal,
31 QC, Canada. H4H 1R3

32

33 * Correspondence: nathan.spren@gmail.com

34

35 Number of Pages: 28

36 Number of Figures: 3

37 Number of Tables: 5

38 Number of Words, Abstract: 240

39 Number of Words, Introduction: 619

40 Number of Words, Discussion: 1444

41

42

JNeurosci Accepted Manuscript

43

44 **Acknowledgements:** This work was supported in part by grants from the Healthy Brains for Healthy
45 Lives, Alzheimer's Association (AARG-22-927100) and NIA R01 AG068563 to R.N.S., who is
46 supported by Fonds de recherche du Québec – Santé. This work was also supported by Canadian
47 Institutes for Health Research (CIHR; #181831) and Fonds de Recherche du Quebec (FRQS; #320680)
48 postdoctoral fellowships to C.S.H.. The PREVENT-AD cohort is supported in part by grants from
49 CIHR (JP, SV), FRQS (JP, SV) and the J.L. Levesque Foundation. Data used in preparation of this
50 article were obtained from the Pre-symptomatic Evaluation of Novel or Experimental Treatments for
51 Alzheimer's Disease (PREVENT-AD) program (<https://douglas.research.mcgill.ca/stop-ad-centre>). A
52 complete listing of the PREVENT-AD Research Group can be found in:

53 [https://preventad.loris.ca/acknowledgements/acknowledgements.php?date=\[2023-07-01\]](https://preventad.loris.ca/acknowledgements/acknowledgements.php?date=[2023-07-01]).

54

55

56

57 **Conflict of Interest:** The authors declare no conflicts

58

59

60

62 **Abstract)**

63 Elevated iron deposition in the brain has been observed in older adult humans and persons with
64 Alzheimer's disease (AD), and has been associated with lower cognitive performance. We investigated
65 the impact of iron deposition, and its topographical distribution across hippocampal subfields and
66 segments (anterior, posterior) measured along its longitudinal axis, on episodic memory in a sample of
67 cognitively unimpaired older adults at elevated familial risk for AD (N = 172, 120 females, 52 males;
68 mean age = 68.8 ± 5.4 y). MRI-based quantitative susceptibility maps were acquired to derive estimates
69 of hippocampal iron deposition. The Mnemonic Similarity Task was used to measure pattern separation
70 and pattern completion, two hippocampally-mediated episodic memory processes. Greater
71 hippocampal iron load was associated with lower pattern separation and higher pattern completion
72 scores, both indicators of poorer episodic memory. Examination of iron levels within hippocampal
73 subfields across its long axis revealed topographic specificity. Among the subfields and segments
74 investigated here, iron deposition in the posterior hippocampal CA1 was most robustly and negatively
75 associated with lower fidelity memory representations. This association remained after controlling for
76 hippocampal volume and was observed in the context of normal performance on standard
77 neuropsychological memory measures. These findings reveal that the impact of iron load on episodic
78 memory performance is not uniform across the hippocampus. Both iron deposition levels as well as its
79 spatial distribution, must be taken into account when examining the relationship between hippocampal
80 iron and episodic memory in older adults at elevated risk for AD.

81

82 **Significance statement**

83 The objective of this study was to map hippocampal iron deposition and its topographical distribution
84 in cognitively unimpaired older adults at risk for AD, and its relationships to hippocampal-mediated
85 episodic memory processes, i.e., pattern separation and pattern completion. Results revealed that
86 elevated hippocampal iron, particularly within the posterior CA1 subfield, was strongly associated with
87 lower pattern separation and higher pattern completion, both markers of poorer episodic memory. This
88 is the first evidence that the spatial distribution of iron deposition in the human hippocampus has
89 specific impacts on memory performance, and may be a more precise early neuropathological marker
90 of insipient memory dysfunction in older adults at elevated risk for AD, but who remain clinically
91 asymptomatic.

92

93 **Keywords:** Quantitative susceptibility mapping; iron; hippocampus; hippocampal subfields; pattern
94 separation; pattern completion; Alzheimer's disease

95

JNeurosci Accepted Manuscript

96 **Introduction**

97 Iron accumulation in the brain is associated with neuropathological changes and
98 neurodegenerative conditions including Alzheimer's disease (AD) (Zecca, 2004; Damulina, 2020;
99 Ayton, 2020; Moon, 2016), potentially promoting β -amyloid toxicity and tau-protein dysfunction
100 through oxidative tissue damage (Ayton, 2015; Ayton, 2021; Cogswell, 2021; Lane, 2018). Elevated
101 iron levels have been observed in the human hippocampus both in normal aging (Bartzokis, 2007;
102 Rodrigue, 2013; Daugherty, 2015) as well as AD (Acosta-Cabronero, 2013; Kim, 2017), suggesting
103 that hippocampal iron may exacerbate the impact of AD-related neuropathology, even before the
104 emergence of a clinical syndrome (Ayton et al., 2017; Chen et al., 2021). As such, hippocampal iron
105 deposition may be an early pathological marker of insipient memory dysfunction in presymptomatic
106 AD.

107 Quantitative Susceptibility Mapping (QSM) is an MRI approach for estimating brain iron levels *in*
108 *vivo* (Lin, Chao, & Wu, 2015). This method, along with earlier relaxometry-based approaches
109 (Bartzokis et al., 2011; Rodrigue, Daugherty, Haacke, & Raz, 2013; Venkatesh, Daugherty, & Bennett,
110 2021), has shown that elevated human hippocampal iron globally is associated with poorer episodic
111 memory in aging, mild cognitive impairment and AD (Ayton, 2017; Chen, 2021). However, the impact
112 of iron distribution across functional subfields and segments of the hippocampus (Poppenk, 2013) has
113 yet to be investigated.

114 Here we collected QSM in a sample of asymptomatic older adults at elevated familial risk for AD
115 (Breitner, Poirier, Etienne, & Leoutsakos, 2016; Tremblay-Mercier et al., 2021). We selected the
116 Mnemonic Similarity Task (MST, Kirwan, 2007; Stark, 2013) as a sensitive and specific assay of
117 pattern separation and completion; two processes central to episodic memory (Hunsaker & Kesner,
118 2013). Pattern separation involves the transformation of overlapping information into orthogonal, non-
119 overlapping, representations, necessary for high fidelity mnemonic encoding (Bakker, 2008; Bakker,
120 2012; Lacy, 2010; Yassa, 2010; Yassa, 2011). Pattern completion involves the 'filling in' of missing
121 features from partial or degraded mnemonic representations, resulting in lower fidelity memory
122 retrieval (Bakker, 2008; Lacy, 2010; Rolls, 2013, for a review). Both memory processes are altered in
123 normal aging, MCI, and AD (Ally, Hussey, Ko, & Molitor, 2013; Bakker, Albert, Krauss, Speck, &
124 Gallagher, 2015; Bakker et al., 2012; Brock Kirwan et al., 2012; Stark, Yassa, Lacy, & Stark, 2013;
125 Yassa et al., 2010).

126 Pattern separation and completion processes have been mapped to specific hippocampal subfields
127 (Stark, 2013), enabling us to test hypotheses regarding the impact of iron distribution across the
128 hippocampus. The dentate gyrus (DG) is implicated in pattern separation (Bakker, 2008; Bakker, 2012;
129 Lacy, 2010; Yassa, 2010; Yassa, 2011), while CA3 has been related to pattern completion (Bakker,
130 2008; Lacy, 2010; Rolls, 2013, for a review). The CA1 subfield has been associated with both pattern
131 separation and completion (Hanert, Pedersen, & Bartsch, 2019). Although the CA4/subiculum has been
132 less directly implicated in pattern separation and completion (Stevenson et al., 2020), it does show
133 significant iron deposition (Spence et al., 2022). Topographical associations with pattern separation and
134 completion have also been reported along segments of the hippocampal long-axis (Poppenk et al.,
135 2013). Evidence from both animal models and human studies suggest that the anterior segment is
136 associated with retention of coarse-grained (global) information, increasing demands on pattern
137 completion at retrieval. In contrast, the posterior segment has been linked to the encoding of local or
138 fine-grained representational detail, necessary for pattern separation (Bogdan & Huang, 2011; Ekstrom,
139 Copara, Isham, Wang, & Yonelinas, 2011; Kjelstrup et al., 2008; McTighe, Mar, Romberg, Bussey, &
140 Saksida, 2009; Morgan, Macevoy, Aguirre, & Epstein, 2011; Stensola et al., 2012). Here we use QSM
141 and MST to relate hippocampal iron and memory performance in older adults to test the prediction that
142 measuring iron deposition *and distribution* across the hippocampus, is necessary to better understand
143 its impact as a pathological marker of emergent memory dysfunction.

144 **Methods and materials**

145 **Study Participants**

146 Participants were recruited from the PREVENT-AD (PRE-symptomatic EVALuation of
147 Experimental or Novel Treatments for AD) dataset, collected at the Douglas Mental Health University
148 Institute in Montreal (Breitner et al., 2016; Tremblay-Mercier et al., 2021). For inclusion in
149 PREVENT-AD, participants had to meet the following eligibility criteria: (1) Parental or ≥ 2 siblings
150 with AD history with diagnosis; (2) age 60 or older (55 to 59 if parental/sibling onset was within 15
151 years of participant's age); (3) cognitively intact with no diagnosable cognitive disorder. Neuroimaging
152 data for the current study was collected on a 3 Tesla Siemens Prisma. All subjects also underwent a
153 battery of neuropsychological tests. Inclusion criteria involved the completion of a QSM MRI scan,
154 anatomical scan and MST neuropsychological testing. Four participants were excluded due to MST
155 outlier performance using an interquartile range outlier calculation (see Hoaglin, 2003). Additionally,

156 after visually inspecting the images, one additional participant was excluded due to a failure in
157 hippocampal segmentation caused by registration issues. The final sample of eligible participants
158 included 172 cognitively unimpaired older adults, including 120 females and 52 males (See Table 1).

159 **Cognitive Assessments**

160 All participants underwent a comprehensive battery of neuropsychological tests on the same day
161 as their MRI scan. See Table 1.

162 *Experimental memory measure.* For our primary analyses we selected the Mnemonic Similarity
163 Task (MST) as it has shown high selectivity in mapping the structure and function of hippocampal
164 subfields to specific memory processes (Yassar and Stark, 2011; Stark, Kirwan, & Stark, 2019).
165 Typical MST administration involves two phases (Stark, 2013). During the incidental encoding phase
166 participants are asked to make judgments about pictures of common, everyday objects (“Is this item
167 commonly found indoors or outdoors?”). Phase two involves a surprise recognition test. Here
168 participants are asked to view a series of pictures and judge whether they are "old" (previously seen
169 targets), "similar" (lure items that are perceptually similar to targets, but were never seen), or "new"
170 (foil items that were perceptually distinct from the targets and never seen). The task also includes a
171 manipulation of lure similarity, wherein lure items may be binned by their degree of similarity to target
172 items, from high to low. Successfully discriminating targets from lures on the MST requires non-
173 overlapping, distinct representations of encoded items, a hallmark of ‘high fidelity’ memory that is
174 dependent upon pattern separation. In contrast, high false recognition rates for lures as targets is
175 evidence for lower fidelity memory representations. These type of MST errors are hypothesized to
176 result from over reliance on pattern completion processes, leading to imprecise memory retrieval, with
177 error rates positively tracking the degree of lure similarity.

178 Here we report bias-corrected measures for behavioral pattern separation (BPS) and behavioral
179 pattern completion (BPC). We adjusted potential response biases previously observed on the MST in
180 older adults as they tend to response “similar” or “old” significantly more. (Budson, 2006, Ally, 2012,
181 Yeung, 2013, and see Ally et al., 2013, for review and detailed formulas for each measure). Bias-
182 corrected BPS scores were calculated in two ways. First, to account for any bias the participant may
183 have in using the “similar” response overall, scores were calculated as the difference between the
184 probabilities of giving a ‘similar’ response to lure versus foil items [similarity-bias corrected BPS
185 score: pattern separation rate minus similar bias rate] (BPS-S; Stark et al., 2013). Second, to account

186 for a general bias towards labelling items as ‘old’, we subtracted the rate of ‘old’ versus ‘similar’
187 responses to lure items [old-bias corrected BPS score: pattern separation rate minus pattern completion
188 rate] (BPS-O; Holden, Toner, Pirogovsky, Kirwan, & Gilbert, 2013; Toner et al., 2009). Bias-corrected
189 BPC scores were derived by subtracting the rate of ‘old’ responses to foil versus lure items [bias-
190 corrected BPC score: pattern completion rate minus false alarm rate].

191 Finally, we calculated a measure to estimate the impact of lure familiarity on memory retrieval
192 (Wilson, Gallagher, Eichenbaum, & Tanila, 2006; Yassa, Mattfeld, et al., 2011). This approach has
193 been used to evaluate the fidelity of memory representations by contrasting the relative influence of
194 pattern separation versus pattern completion during retrieval judgments (Stark et al., 2013; see Yassa,
195 Lacy, et al., 2011, for a review). The measure is an inverse ratio of old versus other responses,
196 calculated across lure similarity bins. An area under the curve estimate was calculated to index the
197 fidelity of memory representations. Higher area under the curve values suggest greater influence of
198 pattern separation versus pattern completion processes at retrieval. We refer to this measure as a
199 memory Fidelity Index (FI) throughout the paper.

200 *Standard clinical memory measures.* While not the focus of the current report, we also conducted
201 exploratory analyses to investigate the impact of hippocampal iron on standard neuropsychological
202 measures of episodic memory collected as part of the PREVENT-AD neurocognitive battery
203 (Tremblay-Mercier et al., 2021). These standard measures are among the most common clinical assays
204 of hippocampally-mediated memory functioning (Wicking, 2014). From the Rey-Auditory Verbal
205 Learning Test (RAVLT; Schmidt, 1996; Moradi et al., 2017) we used immediate recall (sum of trials 1-
206 5), delayed recall, and percentage forgetting (trial 5 score, minus delayed recall score divided by the
207 score of trial 5). From the Repeatable Battery for Assessment of Neuropsychological Status (RBANS,
208 Randolph, 1998) we used the immediate and delayed recall index scores. Three participants failed to
209 complete the RAVLT due to fatigue and were excluded from all analyses involving this test.

210

211

Table 1

A) Demographics	
N	172
Ages(years)	68.8 (5.4)
Sex	
Female	120
Male	52
Education(years)	15.4 (3.3)
APOE genotype	
APOE4 positive	69
APOE4 negative	103
B) Memory measures	
Episodic memory (items recalled)	
RAVLT delay	8.64 (3.79)
RAVTL immediate	48.10 (8.94)
RAVTL percentage forgetting	0.3 (0.27)
RBANS delay	104.03 (10.03)
RBANS immediate	106.58 (12.89)
MST performance	
Pattern Separation	
Similarity- bias corrected BPS score	0.14 (0.15)
Old-bias corrected BPS score	- 0.38 (0.27)

Pattern Completion

Bias-corrected BPC score	0.56 (0.13)
--------------------------	-------------

Memory Fidelity

FI-AUC	2.53 (0.69)
--------	-------------

212

213

214 Table 1. Panel A: Demographic information for study participants [Mean (SD)]. Panel B: Memory
215 scores. RAVLT = Rey Auditory Verbal Learning Test, RBANS = Repeatable Battery for the
216 Assessment of Neuropsychological Status, BPS = behavioral pattern separation, BPC = behavioral
217 pattern completion, FI = Fidelity Index, AUC = Area Under the Curve across seven conditions [Mean
218 (SD)].

219

220

221 Neuroimaging protocols

222 MRI scans were conducted on a Siemens Prisma 3T MRI scanner (Siemens Medical Solutions,
223 Erlangen, Germany) with a 32-channel head coil at the Cerebral Imaging Centre of the Douglas Mental
224 Health University Institute. A 3D spoiled gradient recalled echo sequence (TE=7.29ms; TR=20ms;
225 FOV=230 mm²; Flip angle=15⁰; Voxel resolution=0.8×0.8×1.0 mm³, 6/8 partial Fourier; GRAPPA
226 factor =2; 144 slices; 5.13min acquisition time) was acquired for QSM and a multi-echo field map
227 (TE=4.80ms/9.90ms/15.00ms; TR=20ms; FOV=230 mm²; Voxel resolution=3.6×3.6×4.0 mm³, 6/8
228 partial Fourier; GRAPPA factor =2; 52 slices; 0:38 min). In addition, T1-weighted (T1w) structural
229 images were acquired with a high-resolution magnetization-prepared rapid gradient echo (MP-RAGE)
230 (TR=2300.0ms; TE=2.96ms; FOV=256mm²; Flip angle=9⁰; Voxel resolution=1.0 x 1.0 x 1.0 mm, 192
231 slices; 5:30 min acquisition time), and T2-weighted images (T2w) (TR=2500.0ms; TE=198ms;
232 FOV=206 mm²; Voxel size=0.6 x 0.6 x 0.6 mm; turbo factor=143; 7:35 min acquisition time) (Bussy et
233 al., 2021).

234 Image processing

235 *QSM data processing.* QSM reconstruction involved several core preprocessing steps, summarized
236 in Figure 1. First, we combined the phase images from the 32 channel receiver to calculate offset maps
237 using phase-offset estimation from multi-echo method adapted from (Sun et al., 2020)
238 (https://github.com/sunhongfu/QSM/tree/master/coil_combination) on low resolution field maps. After
239 registration, the offset maps were subtracted from the high-resolution spoiled gradient echo the phase
240 images to obtain offset-corrected phase images without singularities. The corrected phase image and
241 magnitude image were then used for QSM reconstruction. The QSM maps were reconstructed using a
242 total-generalized-variation based method (<http://www.neuroimaging.at/pages/qsm.php>) (Langkammer
243 et al., 2015). This method incorporates the three individual steps involved in common QSM pipelines:
244 phase unwrapping, background field removal, and dipole inversion in a single iteration, which greatly
245 reduces noise and is especially suitable for low SNR data.

246 *Segmentation and quantification of susceptibility.* Hippocampal segmentations were performed
247 using the Automatic Segmentation of Hippocampal Subfields (ASHS) package. Two separate ASHS
248 pipelines were used to derive hippocampal subfield and segment ROIs. To identify subfields, a
249 combined T1w and T2w pipeline for hippocampal subfield segmentation was implemented
250 (Yushkevich et al., 2015). To identify segments, a T1w pipeline for segmenting the long axis of the

251 hippocampus into anterior and posterior regions. Here, anterior hippocampus (aHPC) corresponds to
252 the head, while posterior hippocampus (pHPC) corresponds to the hippocampal body and tail (Xie L.,
253 2016). The anterior and posterior segment ROIs was further used to separate the subfields into anterior
254 and posterior portions. To improve delineation of tissue boundaries in the T1w images, the GRE
255 magnitude images were first linearly coregistered with each individual's T1w, and the T2w images
256 were coregistered with T1w. Finally, the transformation matrices were combined and applied to the
257 QSM map. This was accomplished using FSL image processing tools (Smith et al., 2004) v.6.0.4). All
258 ROIs were visually inspected to ensure quality of anatomical delineation, alignment across
259 neuroimages, and non-overlap of independent ROIs. As we do not have laterality hypotheses, we
260 averaged the left and right ROIs, resulting in combined bilateral measures for the full hippocampus as
261 well as each subfield and segment (see Figure 1). This resulted in nine ROIs: whole hippocampus plus
262 the anterior and posterior CA1, CA3, DG, and subiculum (SUB), selected based on evidence of
263 involvement in pattern separation or completion and/or significant iron deposition (Baker et al., 2016;
264 Brock Kirwan et al., 2012; Hanert et al., 2019; Poppenk, Evensmoen, Moscovitch, & Nadel, 2013;
265 Wilson, Gallagher, Eichenbaum, & Tanila, 2006; Spence McNeil, & Waiter, 2022; Stevenson, Reagh,
266 Chun, Murray, & Yassa, 2020). Median susceptibility values, reflecting iron deposition estimates, were
267 adjusted for subject-wise variability in scan acquisitions by standardizing all hippocampal measures by
268 the median susceptibility value of the corpus callosum. This region is commonly selected as a reference
269 region due to high signal reliability (Bilgic, Pfefferbaum, Rohlfing, Sullivan, & Adalsteinsson, 2012;
270 Meineke et al., 2018)). As such, QSM provides a measure of relative rather than absolute susceptibility
271 (Cheng, Neelavalli, & Haacke, 2009).

272 *Regional volumetry.* Anatomical images were skull stripped using FSL 'bet2' (Smith, 2002).
273 Volumetric segmentation (e.g., corpus callosum and intracranial volume) was completed using the
274 FreeSurfer software suite (Dale, Fischl, & Sereno, 1999) v.7.3.2).

275

276 **Statistical analysis**

277 Hierarchical regression analyses were conducted to examine associations between iron levels and
278 MST scores. Level one incorporated demographic covariates (age, education, and sex) and APOE $\epsilon 4$
279 status (APOE4+/-). Next, intracranial and hippocampal volumes were added to the model to test, and
280 control for, associations between brain volume and MST performance. Finally, whole hippocampal iron
281 deposition values were added to examine whether iron remained a significant contributor to MST
282 performance over and above the contributions of demographics and brain volume. Separate hierarchical
283 regressions were conducted for the four MST scores in four models: Pattern separation (BPS similarity-
284 bias corrected, BPS old-bias corrected); Pattern completion (bias corrected); Fidelity Index (FI-area
285 under the curve). All four models are reported to demonstrate the robustness of the observed effects,
286 regardless of any specific MST score. For this reason, p-value corrections were not applied. To test
287 predictions regarding topographical specificity, we next examined associations between iron deposition
288 and MST independently in six hippocampal subregions (CA1, CA3, DG, subiculum, aHPC, pHPC) using
289 the hierarchical regression approach outlined above. Finally, we combined our hippocampal
290 segmentation techniques to identify posterior and anterior segments of each subfield, resulting in eight
291 independent ROIs (e.g. anterior CA1, posterior CA1, anterior CA3 etc.). For these analyses we
292 performed a series of stepwise regressions for the four MST measures. This approach enabled us to test
293 the specific contributions of iron deposition within each segmented subfield to MST performance. For
294 these analyses, we first residualized each MST explanatory variable for the effects of the control variables
295 (age, education, sex, intracranial volume, whole and segmented hippocampal volumes, and APOE
296 genotype). These residuals were then used as predictors in subsequent stepwise regression models. To
297 evaluate the significance of each model we selected values for probability-of-*F*-to-enter of $\leq .05$ (and
298 probability-of-*F*-to-remove of $\geq .10$) as entry criteria for adding subsequent variables. '*F*-change' values
299 were calculated to measure the amount of extra variance explained from the previous model. To
300 determine the relative contribution of each model predictor to MST performance, we implemented
301 constrained dominance analysis (DA, Azen & Budescu, 2003), which is based on the constrained relative
302 importance analytical approach (LeBreton, Tonidandel, & Krasikova, 2013). The eight explanatory
303 variables (iron values from each ROI) were residualized for the control variables (e.g., age, education,
304 sex, intracranial volume, whole hippocampal volume, specific hippocampal segment volume (e.g.
305 posterior CA1 volume for CA1 iron) and APOE genotype). Next, dominance analysis was used to
306 determine the incremental contribution of each explanatory variable in predicting MST performance,
307 measured as an increase in R^2 associated with adding each predictor to the subset of the remaining

308 predictors. Finally, a Percentage Relative Importance (PRI) value was derived for each predictor by
309 calculating the percentage of dominance value:

310

$$311 \quad [PRI = \frac{\text{average contribution (each predictor)}}{\text{the sum of average contribution (all predictors)}}].$$

312

313 Finally, to investigate associations between hippocampal iron and standard neuropsychological
314 measures of episodic memory (RAVLT and RBANS), we used partial correlation analyses, consistent
315 with previous reports (Ayton, 2017; Chen, 2021). All partial correlation models included sex, age, years
316 of education, intracranial volume, hippocampal (whole and segmented) volumes and APOE genotype as
317 covariates. All statistical analyses were performed using IBM SPSS 28.0 (Armonk, NY, USA) and R
318 (version 4.2.1).

319 **Results**

320 Estimates of QSM values for iron deposition, volume and density for the whole hippocampus,
321 hippocampal subfields and segments and subregions, are reported in Table 2. Correlations among iron
322 levels across the whole hippocampus, segments, and subfields are reported in Figure 2.

323

Table 2

ROIs	Susceptibility(ppm)	Volume(ml)	Iron density (ppm/ml)
Hippocampus	0.035 (0.009)	3781.3 (425.5)	9.26×10^{-6}
CA1	0.035 (0.010)	1215.9 (172.7)	2.88×10^{-5}
CA3	0.009 (0.019)	68.7 (35.1)	1.31×10^{-4}
DG	0.027 (0.011)	730.0 (103.4)	3.70×10^{-5}
SUB	0.059 (0.013)	425.7 (58.4)	1.39×10^{-4}
aHPC	0.042 (0.012)	1725.3 (279.3)	2.43×10^{-5}
pHPC	0.030 (0.010)	1645.4 (175.7)	1.82×10^{-5}
Anterior CA1	0.044 (0.013)	543.7 (112.2)	8.09×10^{-5}
Posterior CA1	0.031 (0.010)	567.1 (77.7)	5.47×10^{-5}
Anterior CA3	0.011 (0.020)	58.3 (15.7)	1.89×10^{-4}
Posterior CA3	0.016 (0.023)	3.0 (1.9)	5.33×10^{-3}
Anterior DG	0.034 (0.014)	367.8 (63.3)	9.24×10^{-5}
Posterior DG	0.022 (0.011)	337.6 (52.5)	6.52×10^{-5}
Anterior SUB	0.065 (0.018)	186.5 (33.5)	3.49×10^{-4}
Posterior SUB	0.051 (0.013)	176.3 (26.8)	2.89×10^{-4}

325

326

327

328

329

Table 2. Susceptibility (iron load), volumes and iron density (susceptibility/volume) for each ROI [Median (SD)].

330 Hippocampal iron and MST performance

331

332 *Whole hippocampus.* Results of the hierarchical regression analyses for MST performance and
333 QSM-derived estimates of iron deposition across the whole hippocampus were consistent with
334 predictions and are reported in Table 3. After controlling for demographic factors as well as hippocampal
335 volume, estimates of hippocampal iron were significantly and negatively associated with similarity-bias
336 and old-bias corrected measures of pattern separation (BPS-S, $\beta=-.18$, $p=.02$; BPS-O, $\beta=-.20$, $p=.01$).
337 In contrast, hippocampal iron was positively associated with bias-corrected pattern completion score;
338 however, the statistical reliability of this association fell below standard, non-directional significance-
339 testing thresholds ($\beta=.14$, $p=.08$). Whole brain hippocampal iron was also negatively associated with the
340 memory fidelity index ($\beta=-.18$, $p=.03$).

JNeurosci Accepted Manuscript

Table 3

	Pattern Separation	Pattern Completion	Memory Fidelity Index
	Similarity-bias corrected BPS score	Old-bias corrected BPS score	Bias-corrected BPC score
	β (CI) (p value)	β (CI) (p value)	β (CI) (p value)
Level1: Demographic variables			
Age	-.29 (-.00, .00) (.002)	-.27 (-.00, .00) (.004)	.08 (.00, .00) (.39)
Education	.07 (-.00, .01) (.34)	.07 (-.01, .02) (.39)	-.01 (-.01, .01) (.88)
Sex	-.19 (-.12, .00) (.04)	-.09 (-.16, .06) (.35)	.09 (-.03, .08) (.36)
APOE4	-.11 (-.08, .01) (.15)	.02 (-.07, .10) (.77)	-.04 (-.05, .03) (.59)
R^2	0.122	0.069	0.01
F	5.827	3.071	0.413
Level 2: Control variables			
TIV	.11 (.00, .00) (.29)	.12 (.00, .00) (.27)	-.14 (.00, .00) (.22)
HC vol	-.07 (.00, .00) (.51)	-.10 (.00, .00) (.36)	.08 (.00, .00) (.50)
R^2	0.126	0.073	0.017

ΔF	0.319	0.392	0.563	0.321
ΔR^2	0.004	0.004	0.007	0.004
Level 3: Variable of interest				
HC iron	-.18 (-5.35, -.55) (.02)	-.20 (-10.06, -1.2) (.01)	.14 (-.23, 4.06) (.08)	-.18 (-24.65, -1.48) (.03)
R^2	0.156	0.107	0.035	0.052
ΔF	5.867	6.298	3.097	4.961
ΔR^2	0.03	0.034	0.018	0.029

Table 3. Results of Hierarchical Regression Analyses for pattern separation and completion and iron level in the whole hippocampus. All standardized regression coefficients (β) are from the level 3 in the analysis (see Text). Data in parentheses are 95% CIs. *P* values less than .05 indicate statistical significance. TIV = Total intracranial volume, HC vol=hippocampus volume, HC = hippocampus.

Hippocampal subfields. Next, we examined associations between MST measures and iron deposition in hippocampal subfields following the hierarchical regression approach described above. Iron levels in CA1 were significantly and negatively related to similarity-bias and old-bias corrected pattern separation scores, controlling for demographic factors, APOE genotype, and structural volume (BPS-S, $\beta = -.20$, $p = .008$; BPS-O, $\beta = -.21$, $p = .007$). In contrast, CA1 iron approached significance in being positively related to the bias-corrected pattern completion scores (bias-corrected BPC, $\beta = .16$, $p = .06$). We also observed a significant and negative association between iron load in CA1 and the memory fidelity index ($\beta = -.19$, $p = .02$). No significant associations were observed for the CA3 and DG subfields. Associations between iron in the SUB and these MST measures followed a similar trend as CA1. SUB iron significantly and negatively correlated with pattern separation scores (BPS-S, $\beta = -.20$, $p = .008$; BPS-O, $\beta = -.22$, $p = .005$), and was negatively associated with memory FI ($\beta = .19$, $p = .02$).

Anterior and posterior hippocampal segments. We next examined associations between MST measures and iron deposition in anterior and posterior hippocampal segments. No significant associations were observed for the anterior hippocampus. As predicted, posterior hippocampal iron levels were negatively and significantly associated with similarity-bias and old-bias corrected pattern separation scores (BPS-S, $\beta = -.17$, $p = .03$; BPS-O, $\beta = -.16$, $p = .04$). Posterior hippocampal iron levels trended towards a negative association with memory FI, ($\beta = -.14$, $p = .07$).

Anterior and posterior hippocampal subfields. To examine our topographical specificity hypotheses further, we conducted stepwise regression analyses to test associations between the anterior and posterior CA1, CA3, DG and SUB subfields and MST measures (see Table 4). All analyses were conducted on residualized susceptibility values after controlling for demographic and structural volume measures. When added to the stepwise regression model, iron deposition in posterior CA1 was the only significant predictor of similarity-bias corrected (BPS-S) scores ($R^2 = .037$, $F_{\text{change}}(1,170) = 6.484$, $p = .012$). Iron deposition levels in posterior subfields CA1 predicted old-bias corrected pattern separation (BPS-O) scores ($R^2 = .038$, $F_{\text{change}}(1,170) = 6.801$, $p = .01$). Additionally, posterior CA1 iron predicted the memory fidelity index ($R^2 = .028$, $F_{\text{change}}(1,170) = 4.820$, $p = .029$) There were no significant predictors of the bias corrected BPC scores (all probabilities of $F_{\text{change}} > p = .1$) (see Table 4 for a summary of all stepwise regression model results).

Finally, constrained dominance analyses revealed that iron deposition in posterior CA1 was the most dominant predictor of performance across all MST measures. Relative contributions of all predictors for each MST score are reported in Figure 3.

JNeurosci Accepted Manuscript

Table 4

Independent variables	Models	Predictors	Standardized β	SE	R ²	<i>P</i> value
Similarity-bias corrected BPS score	1	Posterior CA1	-0.192	0.011	0.037	0.012
Old-bias corrected BPS score	1	Posterior CA1	-0.196	0.02	0.038	0.01
FI-AUC	1	Posterior CA1	-0.166	0.052	0.028	0.029

Table 4. Results of stepwise regression analyses for pattern separation, completion and iron level in the anterior and posterior hippocampal subfields. Residual explanatory variables denoted for posterior CA1. The model for bias-corrected BPC score was non-significant. *P* values less than .05 indicate statistical significance. FI = Memory fidelity index (area under the curve).

Hippocampal iron and standard neuropsychological memory measures

In a series of exploratory analyses, we examined the relationship between performance on standard neuropsychological measures of memory (see Table 1) and hippocampal iron deposition using partial correlation analyses, controlling for demographic variables, APOE4 status and hippocampal volumes. No significant associations emerged for our five memory measures and whole hippocampal iron. Interestingly, at the level of hippocampal segments and subfields, several associations did pass standard statistical significance thresholds ($p < .05$). Consistent with our MST findings, iron deposition in the CA1 subfield, and its posterior aspect specifically, was associated with poorer memory performance. A similar pattern was also observed for posterior DG and the posterior segment of the hippocampus. Notably, iron deposition in the CA3 and anterior CA3 subfield was specifically related to greater percent forgetting on the RAVLT, a measure known to be sensitive to the emergence of clinical AD (Moradi et al., 2017).

Table 5

ROIs	RAVLT $pr(p)$			RBANS $pr(p)$	
	Delay recall	Immediate recall	Percentage forgetting	Delay recall	Immediate recall
Hippocampus	-.11 (.15)	-.06 (.46)	.11 (.15)	-.11 (.15)	-.14 (.07)
CA1	-.11 (.17)	-.07 (.36)	.11 (.18)	-.18 (.02*)	-.18 (.03*)
CA3	-.15 (.05)	-.00 (.99)	.16 (.04*)	-.01 (.89)	-.01 (.87)
DG	-.08 (.29)	-.04 (.60)	.09 (.26)	-.06 (.42)	-.11 (.15)
SUB	-.07 (.36)	-.05 (.49)	.11 (.15)	-.02 (.82)	-.06 (.34)
aHPC	-.12 (.13)	-.03 (.67)	.13 (.11)	-.05 (.52)	-.03 (.74)
pHPC	-.08 (.34)	-.06 (.42)	.07 (.38)	-.14 (.08)	-.20 (.01*)
Anterior CA1	-.12 (.13)	-.04 (.65)	.13 (.09)	-.16 (.04*)	-.09 (.27)
Posterior CA1	-.07 (.35)	-.07 (.39)	.06 (.45)	-.16 (.04*)	-.19 (.02*)
Anterior CA3	-.15 (.05)	-.01 (.94)	.16 (.04*)	-.02 (.78)	-.03 (.71)
Posterior CA3	-.04 (.63)	-.02 (.77)	.03 (.68)	-.02 (.83)	-.12 (.11)
Anterior DG	-.11 (.19)	-.05 (.53)	.12 (.12)	-.01 (.88)	-.01 (.88)

Posterior DG	-.08 (.33)	-.07 (.41)	.07 (.41)	-.15 (.06)	-.21 (.01*)
Anterior SUB	-.06 (.45)	.03 (.68)	.07 (.38)	-.01 (.92)	-.01 (.90)
Posterior SUB	-.06 (.44)	-.01 (.91)	.10 (.20)	-.07 (.36)	-.11 (.15)

Table 5. Results from partial association between iron load and cognitive scores of standard clinical measures of episodic memory. Values for *pr* and *P* are given for each cognitive measure. * indicates $p < .05$, uncorrected. No associations are significant with Bonferroni correction.

Discussion (1444/1500)

We used QSM to investigate the impact of iron deposition and its topographical distribution across the hippocampus on memory functioning in a large cohort of older adults who are elevated familial risk for AD, but remain asymptomatic. We derived measures of iron deposition across the whole hippocampus, within CA1, CA3, DG, and the subiculum as well as within their anterior and posterior hippocampal segments. We used these as predictors of pattern separation and completion, assessed using the Mnemonic Similarity Test. Consistent with predictions, we observed robust negative correlations between hippocampal iron and pattern separation, positive correlations with pattern completion, and an overall negative correlation between iron deposition and the fidelity of memory representations, reflected as greater reliance on pattern completion over pattern separation processes. These associations were independent of hippocampal volume and showed topographical specificity, with iron deposition in the posterior aspect of CA1 displaying the most consistent negative associations with memory fidelity.

Our findings extend two earlier reports using T2* relaxometry in typically aging older adults (Bartzokis et al., 2011; Rodrigue et al., 2013). Bartzokis and colleagues (2011) observed a negative association between global hippocampal T2* relaxation time, a related marker of iron concentration, and performance on standard memory measures. Notably, hippocampal volumes were not modelled in their analyses, leaving open the question of whether iron concentration was an independent predictor of memory performance. Rodrigue and colleagues (2013) explicitly modelled associations between global hippocampal volume, iron concentration, and an index of standard memory measures. They reported that higher hippocampal iron was associated with smaller hippocampal volumes, which together accounted for worse memory ability with age. A negative relationship between hippocampal iron deposition and delayed memory performance on standard memory measures has also been observed when directly accounting for hippocampal volume (Venkatesh et al., 2021). While these reports used relaxometry approaches, QSM methods have also been used to investigate associations between hippocampal iron deposition and memory functioning in normal aging, mild cognitive impairment and AD (Ayton et al.,

2017; Chen et al., 2021). Their findings are largely convergent with the relaxometry studies, implicating iron deposition across the hippocampus in memory decline into older age. We are not aware of any previous studies explicitly examining the topographical specificity of these effects.

In our analyses examining hippocampal subfields and segments, the largest unique effects were observed for iron deposition in CA1, which was associated with lower pattern separation, higher pattern completion and lower overall memory fidelity scores. While CA1 has been implicated in pattern completion (Duncan, Ketz, Inati, & Davachi, 2012; Kumaran & Maguire, 2007), there is emerging evidence for its role in pattern separation (Hanert et al., 2019). However, a leading theoretical account argues for a dual role of the CA1 subfield in pattern separation and completion as a downstream, ‘read-out’ layer from upstream DG/CA3 outputs (Guzowski, Knierim, & Moser, 2004); Knierim et al., 2016; Yassa and Stark, 2011). While speculative, functional disruption related to iron deposition in this ‘read-out’ layer would result in poorer pattern separation at encoding and subsequently greater reliance on pattern completion at retrieval as we observed here. Given that CA1, and its posterior aspect specifically, is the largest of the subfields investigated in the current report, it is perhaps unsurprising it would be the region most susceptible to the impact of neuropathological changes, including iron deposition. Consistent with this idea, CA1 is considered vulnerable to multiple physiological changes in aging and AD including vascular atrophy, resulting in disruptions in endothelial function and iron homeostasis (Buch, Chen, Jella, Ge, & Haacke, 2022), inflammatory impacts on iron-containing microglia (Zeineh et al., 2015) as well as increased iron-related gliosis (Venkatesh et al., 2021) all of which serve to promote iron-related oxidative damage to CA1.

In contrast to CA1, the DG and CA3 subfields have been specifically implicated in pattern separation and pattern completion processes respectively (Marr & Brindley, 1971; McClelland & Goddard, 1996; Rolls, 2013; Rolls & Kesner, 2006; Treves & Rolls, 1994; Yassa and Stark, 2011 for a review). We did not observe predicted associations with CA3 iron and MST (but note our exploratory results for RAVLT percent forgetting in Table 5). This may be an artifact of the comparatively small volume of this subfield, resulting in lower sensitivity of QSM measures to detect reliable associations. Unexpectedly, we did observe an association between subiculum iron and MST performance. While this region has been more reliably implicated in source

memory, as the main output of the hippocampus iron related toxicity is likely to impact many hippocampally-dependent memory processes (Stevenson et al., 2020) More recently, novel QSM separation methods have been identified to reliably separate susceptibility sources in QSM, distinguishing the unique contribution of paramagnetic and diamagnetic susceptibility (Dimov et al., 2022; Shin et al., 2021). Application of these methods will be an important future research direction to enhance the specificity of iron estimates from QSM imaging, as necessary to further interrogate the associations reported here.

To our knowledge, no previous studies have examined hippocampal iron across the long axis of the hippocampus, and impacts on memory function. Our preliminary predictions, hypothesizing greater impact of anterior hippocampal iron on pattern completion and posterior hippocampal iron on pattern separation, were only partially supported. We did not observe any significant associations with pattern completion scores in the anterior segment of the hippocampus. However, consistent with predictions we observed robust (and negative) associations between iron in posterior hippocampus and pattern separation. These topographical associations across the hippocampal long axis likely track with the relative subfield volumes in anterior and posterior segments. In adult humans, CA1-3 subfield volumes are relatively larger in the anterior hippocampus, consistent with its hypothesized role in pattern completion. In contrast, DG volumes are greater in the posterior aspect (Malykhin, Lebel, Coupland, Wilman, & Carter, 2010), which is more strongly implicated in pattern separation. Despite these volume differences in anterior and posterior subfields, posterior CA1 iron remained the strongest independent contributor to pattern separation performance, as well as overall memory fidelity. This finding was further confirmed through the dominance analysis wherein iron with the posterior CA1 subfield was the strongest contributor to MST performance in our participants.

While not the focus of the current study, we failed to observe associations between whole hippocampal iron and performance on standardized memory measures. This was unexpected given that previous studies have demonstrated such associations using both T2* relaxometry and QSM measures of iron in older adult cohorts. However, only one of these earlier studies (Rodrigue et al., 2013) included structural volumes directly in their statistical models. The authors used structural equation modeling to assess the impact of hippocampal iron in the context of volume differences, perhaps accounting for the differences with our findings. We also note

that their memory index was more heavily weighted towards associative memory, which is known to be more strongly related to hippocampal function than the item memory tasks used here. This may account for their observed associations between hippocampal iron concentration and performance on associative memory measures. Interestingly, we did observe associations between performance on standard memory measures and iron deposition at the level of hippocampal subfields and segments. Here again iron deposition in CA1 showed the most reliable and negative associations with memory, however these exploratory findings will need to be replicated and confirmed in future research.

Here we provide novel evidence that hippocampal iron is a pathological marker associated with poorer memory function in older adults who are at elevated risk for AD but who remain cognitively unimpaired. These results provide the first demonstration in humans that it is not only iron deposition, but its topographic distribution across hippocampal subfields and segments that determine the pattern of memory dysfunction. These findings open a new avenue and provide strong evidence pointing to the importance of iron deposition as both a mechanism and marker of cognitive dysfunction in later life. Iron deposition in CA1 may be a particularly robust marker of memory dysfunction and an important target for new studies testing the topographic specificity hypothesis. The use of iron chelation therapy, employing agents like deferoxamine, holds potential for alleviating iron levels in specific brain regions of individuals with AD. This approach aims to mitigate or even treat AD, underscoring the significance of iron-targeted therapeutic strategies (Liu et al., 2018). Focusing on addressing iron deposition in particular brain areas, including CA1, may have potential for therapeutic interventions. Finally, this work offers a roadmap for future investigations, highlighting the importance of precision brain and behavioral mapping to reveal the often-subtle associations between pathological markers and behavioral performance in cognitively normal older adults. This may be particularly critical for revealing early neuropathological markers in older adults who are at elevated risk for brain disease, yet are clinically asymptomatic.

References

- Acosta-Cabronero, J., Williams, G. B., Cardenas-Blanco, A., Arnold, R. J., Lupson, V., & Nestor, P. J. (2013). In vivo quantitative susceptibility mapping (QSM) in Alzheimer's disease. *PLoS One*, 8(11), e81093. doi:10.1371/journal.pone.0081093
- Ally, B. A. (2012). Using pictures and words to understand recognition memory deterioration in amnesic mild cognitive impairment and Alzheimer's disease: a review. *Curr Neurol Neurosci Rep*, 12(6), 687-694. doi:10.1007/s11910-012-0310-7
- Ally, B. A., Hussey, E. P., Ko, P. C., & Molitor, R. J. (2013). Pattern separation and pattern completion in Alzheimer's disease: evidence of rapid forgetting in amnesic mild cognitive impairment. *Hippocampus*, 23(12), 1246-1258. doi:10.1002/hipo.22162
- Ayton, S., Faux, N. G., Bush, A. I., & Alzheimer's Disease Neuroimaging, I. (2015). Ferritin levels in the cerebrospinal fluid predict Alzheimer's disease outcomes and are regulated by APOE. *Nat Commun*, 6, 6760. doi:10.1038/ncomms7760
- Ayton, S., Fazlollahi, A., Bourgeat, P., Raniga, P., Ng, A., Lim, Y. Y., . . . Bush, A. I. (2017). Cerebral quantitative susceptibility mapping predicts amyloid-beta-related cognitive decline. *Brain*, 140(8), 2112-2119. doi:10.1093/brain/awx137
- Ayton, S., Portbury, S., Kalinowski, P., Agarwal, P., Diouf, I., Schneider, J. A., . . . Bush, A. I. (2021). Regional brain iron associated with deterioration in Alzheimer's disease: A large cohort study and theoretical significance. *Alzheimer's & Dementia*, 17(7), 1244-1256. doi:https://doi.org/10.1002/alz.12282
- Ayton, S., Wang, Y., Diouf, I., Schneider, J. A., Brockman, J., Morris, M. C., & Bush, A. I. (2020). Brain iron is associated with accelerated cognitive decline in people with Alzheimer pathology. *Mol Psychiatry*, 25(11), 2932-2941. doi:10.1038/s41380-019-0375-7
- Azen, R., & Budescu, D. V. (2003). The dominance analysis approach for comparing predictors in multiple regression. *Psychol Methods*, 8(2), 129-148. doi:10.1037/1082-989x.8.2.129
- Baker, S., Vieweg, P., Gao, F., Gilboa, A., Wolbers, T., Black, S. E., & Rosenbaum, R. S. (2016). The Human Dentate Gyrus Plays a Necessary Role in Discriminating New Memories. *Curr Biol*, 26(19), 2629-2634. doi:10.1016/j.cub.2016.07.081
- Bakker, A., Albert, M. S., Krauss, G., Speck, C. L., & Gallagher, M. (2015). Response of the medial temporal lobe network in amnesic mild cognitive impairment to therapeutic intervention assessed by fMRI and memory task performance. *Neuroimage Clin*, 7, 688-698. doi:10.1016/j.nicl.2015.02.009
- Bakker, A., Kirwan, C. B., Miller, M., & Stark, C. E. L. (2008). Pattern separation in the human hippocampal CA3 and dentate gyrus. *Science*, 319(5870), 1640-1642.
- Bakker, A., Krauss, G. L., Albert, M. S., Speck, C. L., Jones, L. R., Stark, C. E., . . . Gallagher, M. (2012). Reduction of hippocampal hyperactivity improves cognition in amnesic mild cognitive impairment. *Neuron*, 74(3), 467-474. doi:10.1016/j.neuron.2012.03.023

- Bartzokis, G., Lu, P. H., & Mintz, J. (2007). Human brain myelination and amyloid beta deposition in Alzheimer's disease. *Alzheimer's & Dementia*, 3(2), 122-125. doi:<https://doi.org/10.1016/j.jalz.2007.01.019>
- Bartzokis, G., Lu, P. H., Tingus, K., Peters, D. G., Amar, C. P., Tishler, T. A., . . . Connor, J. R. (2011). Gender and iron genes may modify associations between brain iron and memory in healthy aging. *Neuropsychopharmacology*, 36(7), 1375-1384. doi:10.1038/npp.2011.22
- Berron, D., Schutze, H., Maass, A., Cardenas-Blanco, A., Kuijf, H. J., Kumaran, D., & Duzel, E. (2016). Strong Evidence for Pattern Separation in Human Dentate Gyrus. *J Neurosci*, 36(29), 7569-7579. doi:10.1523/JNEUROSCI.0518-16.2016
- Bettio, L. E. B., Rajendran, L., & Gil-Mohapel, J. (2017). The effects of aging in the hippocampus and cognitive decline. *Neurosci Biobehav Rev*, 79, 66-86. doi:10.1016/j.neubiorev.2017.04.030
- Bilgic, B., Pfefferbaum, A., Rohlfing, T., Sullivan, E. V., & Adalsteinsson, E. (2012). MRI estimates of brain iron concentration in normal aging using quantitative susceptibility mapping. *Neuroimage*, 59(3), 2625-2635. doi:10.1016/j.neuroimage.2011.08.077
- Boggan, A. L., & Huang, C. M. (2011). Chess expertise and the fusiform face area: why it matters. *J Neurosci*, 31(47), 16895-16896. doi:10.1523/jneurosci.4689-11.2011
- Breitner, J. C. S., Poirier, J., Etienne, P. E., & Leoutsakos, J. M. (2016). Rationale and Structure for a New Center for Studies on Prevention of Alzheimer's Disease (StoP-AD). *J Prev Alzheimers Dis*, 3(4), 236-242. doi:10.14283/jpad.2016.121
- Brock Kirwan, C., Hartshorn, A., Stark, S. M., Goodrich-Hunsaker, N. J., Hopkins, R. O., & Stark, C. E. (2012). Pattern separation deficits following damage to the hippocampus. *Neuropsychologia*, 50(10), 2408-2414. doi:10.1016/j.neuropsychologia.2012.06.011
- Buch, S., Chen, Y., Jella, P., Ge, Y., & Haacke, E. M. (2022). Vascular mapping of the human hippocampus using Ferumoxytol-enhanced MRI. *Neuroimage*, 250, 118957. doi:10.1016/j.neuroimage.2022.118957
- Budson, A. E., Wolk, D. A., Chong, H., & Waring, J. D. (2006). Episodic memory in Alzheimer's disease: separating response bias from discrimination. *Neuropsychologia*, 44(12), 2222-2232. doi:10.1016/j.neuropsychologia.2006.05.024
- Bussy, A., Plitman, E., Patel, R., Tullo, S., Salaciak, A., Bedford, S. A., . . . Chakravarty, M. M. (2021). Hippocampal subfield volumes across the healthy lifespan and the effects of MR sequence on estimates. *Neuroimage*, 233, 117931. doi:<https://doi.org/10.1016/j.neuroimage.2021.117931>
- Chen, L., Soldan, A., Oishi, K., Faria, A., Zhu, Y., Albert, M., . . . Li, X. (2021). Quantitative Susceptibility Mapping of Brain Iron and beta-Amyloid in MRI and PET Relating to Cognitive Performance in Cognitively Normal Older Adults. *Radiology*, 298(2), 353-362. doi:10.1148/radiol.2020201603
- Cheng, Y. C., Neelavalli, J., & Haacke, E. M. (2009). Limitations of calculating field distributions and magnetic susceptibilities in MRI using a Fourier based method. *Phys Med Biol*, 54(5), 1169-1189. doi:10.1088/0031-9155/54/5/005

- Cogswell, P. M., Wiste, H. J., Senjem, M. L., Gunter, J. L., Weigand, S. D., Schwarz, C. G., . . . Jack, C. R., Jr. (2021). Associations of quantitative susceptibility mapping with Alzheimer's disease clinical and imaging markers. *Neuroimage*, 224, 117433. doi:10.1016/j.neuroimage.2020.117433
- Dale, A. M., Fischl, B., & Sereno, M. I. (1999). Cortical surface-based analysis. I. Segmentation and surface reconstruction. *Neuroimage*, 9(2), 179-194. doi:10.1006/nimg.1998.0395
- Damulina, A., Pirpamer, L., Soellradl, M., Sackl, M., Tinauer, C., Hofer, E., . . . Langkammer, C. (2020). Cross-sectional and Longitudinal Assessment of Brain Iron Level in Alzheimer Disease Using 3-T MRI. *Radiology*, 296(3), 619-626. doi:10.1148/radiol.2020192541
- Daugherty, A. M., & Raz, N. (2015). Appraising the Role of Iron in Brain Aging and Cognition: Promises and Limitations of MRI Methods. *Neuropsychol Rev*, 25(3), 272-287. doi:10.1007/s11065-015-9292-y
- Davachi, L. (2006). Item, context and relational episodic encoding in humans. *Curr Opin Neurobiol*, 16(6), 693-700. doi:10.1016/j.conb.2006.10.012
- Dimov, A. V., Nguyen, T. D., Gillen, K. M., Marcille, M., Spincemaille, P., Pitt, D., . . . Wang, Y. (2022). Susceptibility source separation from gradient echo data using magnitude decay modeling. *J Neuroimaging*, 32(5), 852-859. doi:10.1111/jon.13014
- Duncan, K., Ketz, N., Inati, S. J., & Davachi, L. (2012). Evidence for area CA1 as a match/mismatch detector: A high-resolution fMRI study of the human hippocampus. *Hippocampus*, 22(3), 389-398. doi:https://doi.org/10.1002/hipo.20933
- Eichenbaum, H. (2004). Hippocampus: cognitive processes and neural representations that underlie declarative memory. *Neuron*, 44(1), 109-120. doi:10.1016/j.neuron.2004.08.028
- Ekstrom, A. D., Copara, M. S., Isham, E. A., Wang, W.-c., & Yonelinas, A. P. (2011). Dissociable networks involved in spatial and temporal order source retrieval. *Neuroimage*, 56(3), 1803-1813. doi:https://doi.org/10.1016/j.neuroimage.2011.02.033
- Gallagher, M., Colantuoni, C., Eichenbaum, H., Haberman, R. P., Rapp, P. R., Tanila, H., & Wilson, I. A. (2006). Individual differences in neurocognitive aging of the medial temporal lobe. *Age (Dordr)*, 28(3), 221-233. doi:10.1007/s11357-006-9017-5
- Gómez-Isla, T., Price, J. L., Mckeel, D. W., Morris, J. C., Growdon, J. H., & Hyman, B. T. (1996). Profound loss of layer II entorhinal cortex neurons occurs in very mild Alzheimer's disease. *J Neurosci*, 16(14), 4491-4500.
- Guzowski, J. F., Knierim, J. J., & Moser, E. I. (2004). Ensemble dynamics of hippocampal regions CA3 and CA1. *Neuron*, 44(4), 581-584. doi:10.1016/j.neuron.2004.11.003
- Hanert, A., Pedersen, A., & Bartsch, T. (2019). Transient hippocampal CA1 lesions in humans impair pattern separation performance. *Hippocampus*, 29(8), 736-747. doi:10.1002/hipo.23073
- Hoaglin, D. C. (2003). John W. Tukey and Data Analysis. *Statistical Science*, 18(3), 311-318.
- Holden, H. M., Toner, C., Pirogovsky, E., Kirwan, C. B., & Gilbert, P. E. (2013). Visual object pattern separation varies in older adults. *Learn Mem*, 20(7), 358-362. doi:10.1101/lm.030171.112

- Hunsaker, M. R., & Kesner, R. P. (2013). The operation of pattern separation and pattern completion processes associated with different attributes or domains of memory. *Neurosci Biobehav Rev*, 37(1), 36-58. doi:10.1016/j.neubiorev.2012.09.014
- Kim, H. G., Park, S., Rhee, H. Y., Lee, K. M., Ryu, C. W., Rhee, S. J., . . . Jahng, G. H. (2017). Quantitative susceptibility mapping to evaluate the early stage of Alzheimer's disease. *Neuroimage Clin*, 16, 429-438. doi:10.1016/j.nicl.2017.08.019
- Kirwan, C. B., & Stark, C. E. (2007). Overcoming interference: an fMRI investigation of pattern separation in the medial temporal lobe. *Learn Mem*, 14(9), 625-633. doi:10.1101/lm.663507
- Kjelstrup, K. B., Solstad, T., Brun, V. H., Hafting, T., Leutgeb, S., Witter, M. P., . . . Moser, M. B. (2008). Finite scale of spatial representation in the hippocampus. *Science*, 321(5885), 140-143. doi:10.1126/science.1157086
- Knierim, J. J., & Neunuebel, J. P. (2016). Tracking the flow of hippocampal computation: Pattern separation, pattern completion, and attractor dynamics. *Neurobiol Learn Mem*, 129, 38-49. doi:10.1016/j.nlm.2015.10.008
- Kumaran, D., & Maguire, E. A. (2007). Match–Mismatch Processes Underlie Human Hippocampal Responses to Associative Novelty. *The Journal of Neuroscience*, 27(32), 8517-8524. doi:10.1523/jneurosci.1677-07.2007
- Lacy, J. W., Yassa, M. A., Stark, S. M., Muftuler, L. T., & Stark, C. E. L. (2010). Distinct pattern separation related transfer functions in human CA3/dentate and CA1 revealed using high-resolution fMRI and variable mnemonic similarity. *Learn Mem*, 18(1), 15-18. doi:10.1101/lm.1971110
- 10.1101/lm.1971110.18:15-18
- Lane, D. J. R., Ayton, S., & Bush, A. I. (2018). Iron and Alzheimer's Disease: An Update on Emerging Mechanisms. *J Alzheimers Dis*, 64(s1), S379-S395. doi:10.3233/JAD-179944
- Langkammer, C., Bredies, K., Poser, B. A., Barth, M., Reishofer, G., Fan, A. P., . . . Ropele, S. (2015). Fast quantitative susceptibility mapping using 3D EPI and total generalized variation. *Neuroimage*, 111, 622-630. doi:https://doi.org/10.1016/j.neuroimage.2015.02.041
- LeBreton, J. M., Tonidandel, S., & Krasikova, D. V. (2013). Residualized Relative Importance Analysis. *Organizational Research Methods*, 16(3), 449-473. doi:10.1177/1094428113481065
- Liu, J. L., Fan, Y. G., Yang, Z. S., Wang, Z. Y., & Guo, C. (2018). Iron and Alzheimer's Disease: From Pathogenesis to Therapeutic Implications. *Front Neurosci*, 12, 632. doi:10.3389/fnins.2018.00632
- Malykhin, N. V., Lebel, R. M., Coupland, N. J., Wilman, A. H., & Carter, R. (2010). In vivo quantification of hippocampal subfields using 4.7 T fast spin echo imaging. *Neuroimage*, 49(2), 1224-1230. doi:https://doi.org/10.1016/j.neuroimage.2009.09.042
- Marr, D., & Brindley, G. S. (1971). Simple memory: a theory for archicortex. *Philosophical Transactions of the Royal Society of London. B, Biological Sciences*, 262(841), 23-81. doi:doi:10.1098/rstb.1971.0078
- McClelland, J. L., & Goddard, N. H. (1996). Considerations arising from a complementary learning systems perspective on hippocampus and neocortex. *Hippocampus*, 6(6), 654-665. doi:https://doi.org/10.1002/(SICI)1098-1063(1996)6:6<654::AID-HIPO8>3.0.CO;2-G

- McTighe, S. M., Mar, A. C., Romberg, C., Bussey, T. J., & Saksida, L. M. (2009). A new touchscreen test of pattern separation: effect of hippocampal lesions. *NeuroReport*, 20(9), 881-885. doi:10.1097/WNR.0b013e32832c5eb2
- Meineke, J., Wenzel, F., De Marco, M., Venneri, A., Blackburn, D. J., Teh, K., . . . Katscher, U. (2018). Motion artifacts in standard clinical setting obscure disease-specific differences in quantitative susceptibility mapping. *Phys Med Biol*, 63(14), 14NT01. doi:10.1088/1361-6560/aacc52
- Moon, Y., Han, S. H., & Moon, W. J. (2016). Patterns of Brain Iron Accumulation in Vascular Dementia and Alzheimer's Dementia Using Quantitative Susceptibility Mapping Imaging. *J Alzheimers Dis*, 51(3), 737-745. doi:10.3233/JAD-151037
- Moradi, E., Hallikainen, I., Hanninen, T., Tohka, J., & Alzheimer's Disease Neuroimaging, I. (2017). Rey's Auditory Verbal Learning Test scores can be predicted from whole brain MRI in Alzheimer's disease. *Neuroimage Clin*, 13, 415-427. doi:10.1016/j.nicl.2016.12.011
- Morgan, L. K., Macevoy, S. P., Aguirre, G. K., & Epstein, R. A. (2011). Distances between real-world locations are represented in the human hippocampus. *J Neurosci*, 31(4), 1238-1245. doi:10.1523/jneurosci.4667-10.2011
- Poppenk, J., Evensmoen, H. R., Moscovitch, M., & Nadel, L. (2013). Long-axis specialization of the human hippocampus. *Trends Cogn Sci*, 17(5), 230-240. doi:10.1016/j.tics.2013.03.005
- Price, J. L., Ko, A. I., Ward, M. J., Tsou, S. K., Mckeel, D. W., & Morris, J. C. (2001). Neuron number in the entorhinal cortex and CA1 in preclinical Alzheimer disease. *Arch Neurol*, 58(9), 1395-1402
- Randolph, C., Tierney, M. C., Mohr, E., & Chase, T. N. (1998). The Repeatable Battery for the Assessment of Neuropsychological Status (RBANS): preliminary clinical validity. *J Clin Exp Neuropsychol*, 20(3), 310-319. doi:10.1076/jcen.20.3.310.823
- Rodrigue, K. M., Daugherty, A. M., Haacke, E. M., & Raz, N. (2013). The role of hippocampal iron concentration and hippocampal volume in age-related differences in memory. *Cereb Cortex*, 23(7), 1533-1541. doi:10.1093/cercor/bhs139
- Rolls, E. T., & Kesner, R. P. (2006). A computational theory of hippocampal function, and empirical tests of the theory. *Prog Neurobiol*, 79(1), 1-48. doi:10.1016/j.pneurobio.2006.04.005
- Rolls, E. T. (2013). The mechanisms for pattern completion and pattern separation in the hippocampus. *Front Syst Neurosci*, 7, 74. doi:10.3389/fnsys.2013.00074
- Schmidt, M. (1996). *Rey Auditory and Verbal Learning Test. A handbook*. Los Angeles: Western Psychological Association.
- Shin, H.-G., Lee, J., Yun, Y. H., Yoo, S. H., Jang, J., Oh, S.-H., . . . Lee, J. (2021). χ -separation: Magnetic susceptibility source separation toward iron and myelin mapping in the brain. *Neuroimage*, 240, 118371. doi:https://doi.org/10.1016/j.neuroimage.2021.118371
- Smith, S. M. (2002). Fast robust automated brain extraction. *Human Brain Mapping*, 17(3), 143-155. doi:https://doi.org/10.1002/hbm.10062

- Spence, H., McNeil, C. J., & Waiter, G. D. (2022). Cognition and brain iron deposition in whole grey matter regions and hippocampal subfields. *Eur J Neurosci*, 56(11), 6039-6054. doi:10.1111/ejn.15838
- Stark, S. M., Yassa, M. A., Lacy, J. W., & Stark, C. E. (2013). A task to assess behavioral pattern separation (BPS) in humans: Data from healthy aging and mild cognitive impairment. *Neuropsychologia*, 51(12), 2442-2449. doi:10.1016/j.neuropsychologia.2012.12.014
- Stark, S. M., Yassa, M. A., & Stark, C. E. (2010). Individual differences in spatial pattern separation performance associated with healthy aging in humans. *Learn Mem*, 17(6), 284-288. doi:10.1101/lm.1768110
- Stensola, H., Stensola, T., Solstad, T., Frøland, K., Moser, M.-B., & Moser, E. I. (2012). The entorhinal grid map is discretized. *Nature*, 492(7427), 72-78. doi:10.1038/nature11649
- Stevenson, R. F., Reagh, Z. M., Chun, A. P., Murray, E. A., & Yassa, M. A. (2020). Pattern Separation and Source Memory Engage Distinct Hippocampal and Neocortical Regions during Retrieval. *J Neurosci*, 40(4), 843-851. doi:10.1523/JNEUROSCI.0564-19.2019
- Sun, H., Cleary, J. O., Glarin, R., Kolbe, S. C., Ordidge, R. J., Moffat, B. A., & Pike, G. B. (2020). Extracting more for less: multi-echo MP2RAGE for simultaneous T1-weighted imaging, T1 mapping, R2* mapping, SWI, and QSM from a single acquisition. *Magn Reson Med*, 83(4), 1178-1191. doi:10.1002/mrm.27975
- Toner, C. K., Pirogovsky, E., Kirwan, C. B., & Gilbert, P. E. (2009). Visual object pattern separation deficits in nondemented older adults. *Learn Mem*, 16(5), 338-342. doi:10.1101/lm.1315109
- Tremblay-Mercier, J., Madjar, C., Das, S., Pichet Binette, A., Dyke, S. O. M., Etienne, P., . . . Group, P.-A. R. (2021). Open science datasets from PREVENT-AD, a longitudinal cohort of pre-symptomatic Alzheimer's disease. *Neuroimage Clin*, 31, 102733. doi:10.1016/j.nicl.2021.102733
- Treves, A., & Rolls, E. T. (1994). Computational analysis of the role of the hippocampus in memory. *Hippocampus*, 4(3), 374-391. doi:https://doi.org/10.1002/hipo.450040319
- Venkatesh, A., Daugherty, A. M., & Bennett, I. J. (2021). Neuroimaging measures of iron and gliosis explain memory performance in aging. *Hum Brain Mapp*, 42(17), 5761-5770. doi:10.1002/hbm.25652
- Wicking, M., Nees, F., & Steiger, F. (2014). Neuropsychological measures of hippocampal function. *Front Neurol Neurosci*, 34, 60-70. doi:10.1159/000356425
- Wilson, I. A., Gallagher, M., Eichenbaum, H., & Tanila, H. (2006). Neurocognitive aging: prior memories hinder new hippocampal encoding. *Trends Neurosci*, 29(12), 662-670. doi:10.1016/j.tins.2006.10.002
- Xie L., W. L. E. M., Manjon J.V., Wang H., Das R.S., Wolk D.A., Yushkevich P.A. (2016). Medical Image Computing and Computer-Assisted Intervention – MICCAI 2016. 564-571.
- Yassa, M. A., Lacy, J. W., Stark, S. M., Albert, M. S., Gallagher, M., & Stark, C. E. (2011). Pattern separation deficits associated with increased hippocampal CA3 and dentate gyrus activity in nondemented older adults. *Hippocampus*, 21(9), 968-979. doi:10.1002/hipo.20808

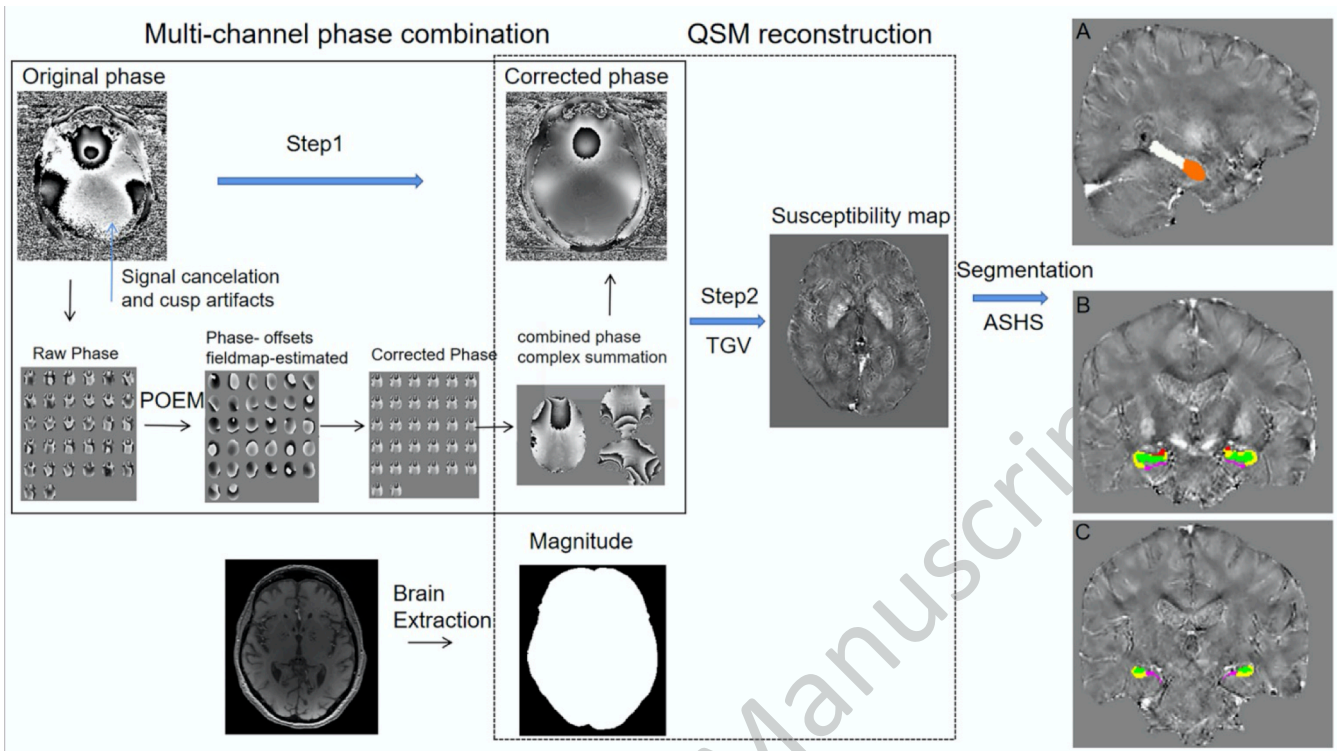
- Yassa, M. A., Mattfeld, A. T., Stark, S. M., & Stark, C. E. L. (2011). Age-related memory deficits linked to circuit-specific disruptions in the hippocampus. *Proceedings of the National Academy of Sciences*, 108(21), 8873-8878. doi:10.1073/pnas.1101567108
- Yassa, M. A., & Stark, C. E. (2011). Pattern separation in the hippocampus. *Trends Neurosci*, 34(10), 515-525. doi:10.1016/j.tins.2011.06.006
- Yassa, M. A., Stark, S. M., Bakker, A., Albert, M. S., Gallagher, M., & Stark, C. E. (2010). High-resolution structural and functional MRI of hippocampal CA3 and dentate gyrus in patients with amnesic Mild Cognitive Impairment. *Neuroimage*, 51(3), 1242-1252. doi:10.1016/j.neuroimage.2010.03.040
- Yeung, L. K., Ryan, J. D., Cowell, R. A., & Barense, M. D. (2013). Recognition memory impairments caused by false recognition of novel objects. *J Exp Psychol Gen*, 142(4), 1384-1397. doi:10.1037/a0034021
- Yushkevich, P. A., Pluta, J. B., Wang, H., Xie, L., Ding, S.-L., Gertje, E. C., . . . Wolk, D. A. (2015). Automated volumetry and regional thickness analysis of hippocampal subfields and medial temporal cortical structures in mild cognitive impairment. *Human Brain Mapping*, 36(1), 258-287. doi:https://doi.org/10.1002/hbm.22627
- Zecca, L., Youdim, M. B., Riederer, P., Connor, J. R., & Crichton, R. R. (2004). Iron, brain ageing and neurodegenerative disorders. *Nat Rev Neurosci*, 5(11), 863-873. doi:10.1038/nrn1537
- Zeineh, M. M., Chen, Y., Kitzler, H. H., Hammond, R., Vogel, H., & Rutt, B. K. (2015). Activated iron-containing microglia in the human hippocampus identified by magnetic resonance imaging in Alzheimer disease. *Neurobiol Aging*, 36(9), 2483-2500. doi:10.1016/j.neurobiolaging.2015.05.022

Figure Captions

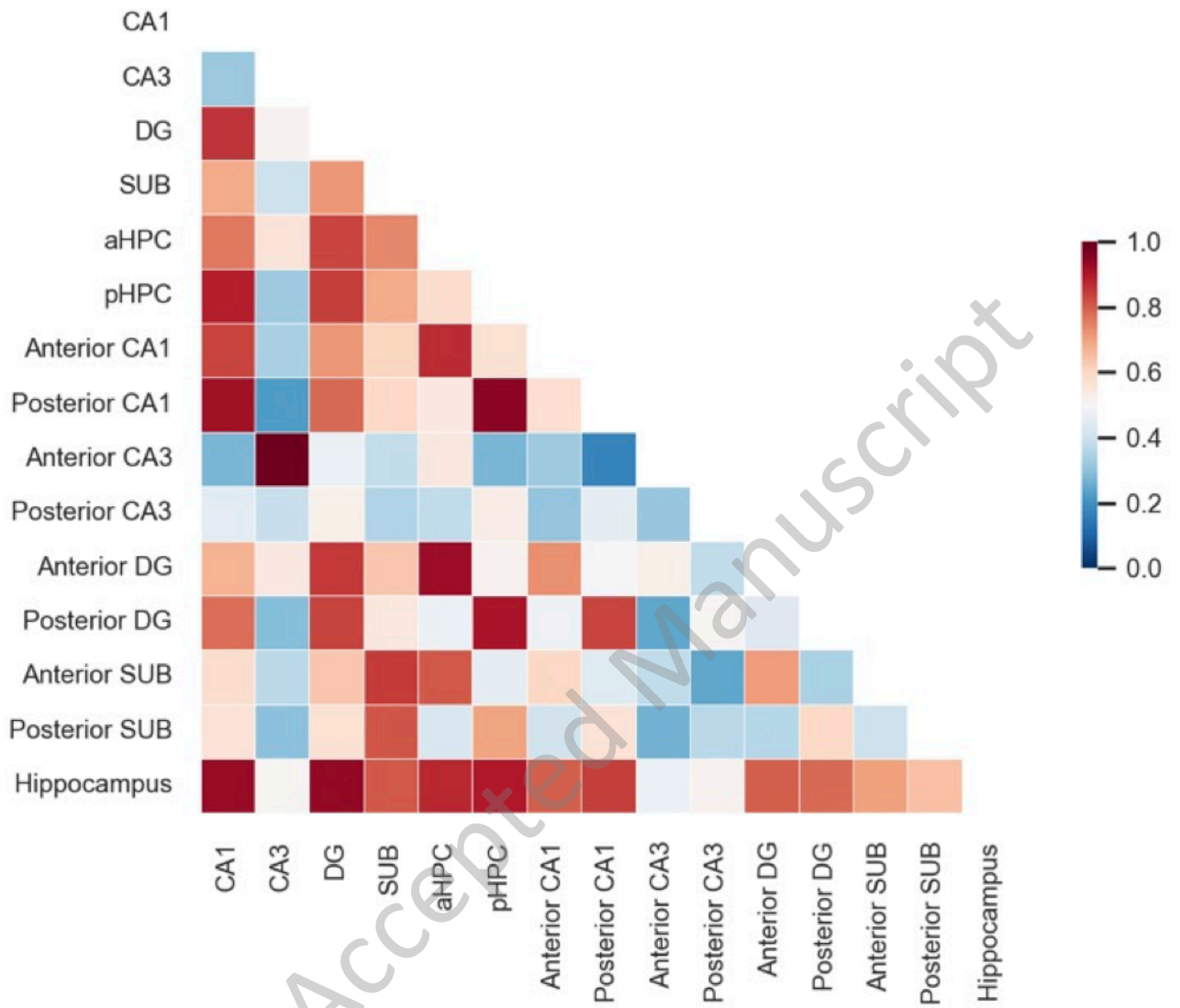
Figure 1 Caption. Schematics for QSM data processing. Step 1: Phase-offset estimation from multi-echo (POEM) applied to correct the phase image. Step 2: Total generalized variation (TGV) method was applied to complete QSM reconstruction. Finally, hippocampal segmentation was performed using Automatic Segmentation of Hippocampal Subfields (ASHS). Far right panel: ASHS outputs overlaid on QSM maps. Panel A: anterior (orange) and posterior (pink) hippocampus; panel B (anterior subfield): anterior CA1 (yellow), anterior CA3 (red), anterior DG (green), anterior SUB (purple); panel C (posterior subfield): posterior CA1 (yellow), posterior CA3 (red) posterior DG (green) and posterior SUB (purple).

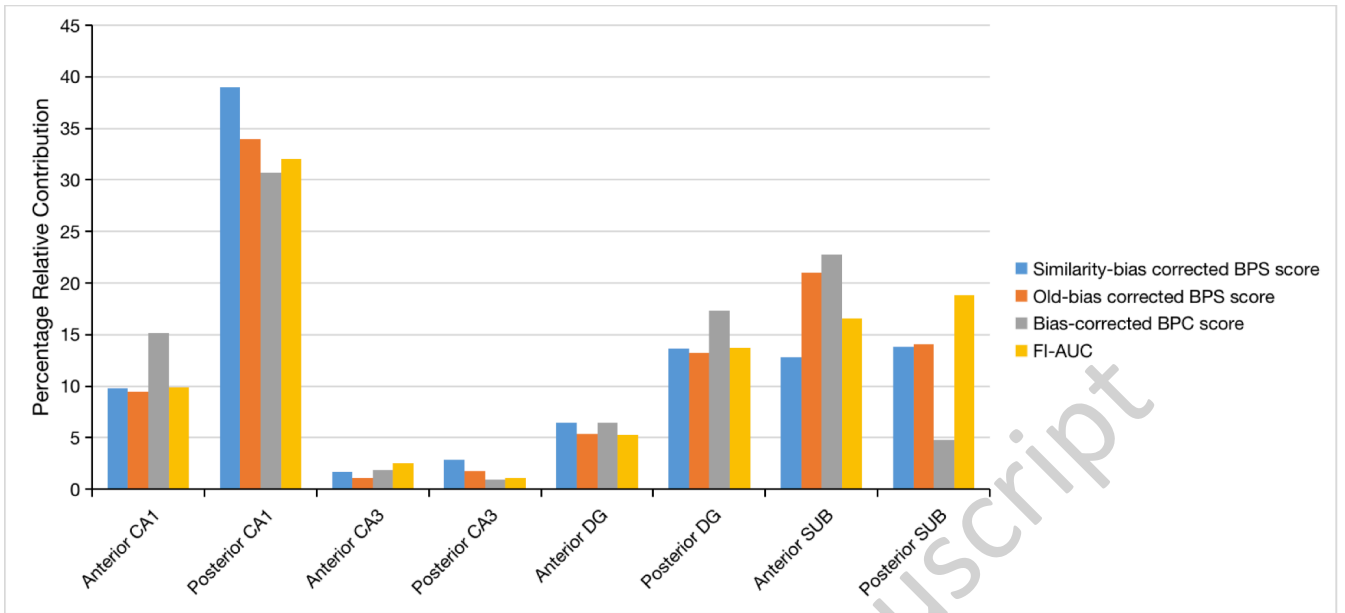
Figure 2 Caption. Heatmap of product-moment correlations between iron measures of the whole hippocampus, anterior and posterior hippocampal segments, hippocampal subfields, and hippocampal subfields split by segment. Each square represents the coefficient value. All p's < .05, uncorrected. Regions are averaged across the left and right hemispheres.

Figure 3 Caption. Constrained dominance analyses. PRI calculated the percentage relative contribution of the independent subregions of anterior and posterior hippocampal subfields to MST cognitive performance. For each cognitive score, the percentage relative contribution of six predictors consisting of residual explanatory variables anterior CA1, posterior CA1, anterior CA3, posterior CA3, anterior DG, posterior DG and anterior SUB and posterior SUB are shown. Iron deposition in posterior CA1 consistently contributes more to explained variance in MST performance relative to other subregions. Note, we first residualized each explanatory variable for the effects of the control variables (age, education, sex, intracranial volume, hippocampal and segmented volume, APOE genotype). FI = Memory fidelity index (area under the curve).



JNeurosci Accepted Manuscript





JNeurosci Accepted Manuscript